Inverse Problems and Imaging
Volume 3, No. 3, 2009, 389–403
doi:10.3934/ipi.2009.3.389

RECIPROCITY GAP MUSIC IMAGING FOR AN INVERSE SCATTERING PROBLEM IN TWO-LAYERED MEDIA

Roland Griesmaier

Department of Mathematical Sciences
University of Delaware
Newark, Delaware 19716, USA

(Communicated by David Colton)

Abstract. In this work we consider a modified MUSIC method for determining the positions of a collection of small perfectly conducting buried objects from measurements of time-harmonic electromagnetic fields on the surface of ground. This method is based on an asymptotic analysis of certain integrals of electric and magnetic fields, so-called reciprocity gap functionals, as the buried objects shrink to points. Unlike standard MUSIC reconstruction methods our algorithm avoids the computation of the Green's function for the background medium during the reconstruction process, but on the other hand it requires more measurement data. After describing the theoretical foundation of this reconstruction method, we provide numerical results showing its performance. We also compare these results to reconstructions obtained by a standard MUSIC algorithm.

1. **Introduction.** The electromagnetic exploration of the ground's subsurface to detect and identify buried objects has drawn increasing attention in recent years, also due to its important applications such as, e.g., humanitarian demining. In the present work we investigate a reconstruction method for an inverse scattering problem arising in this context. We consider a simplified but fully three dimensional model and assume that a collection of small perfectly conducting objects is buried in the lower half space of an unbounded two-layered background medium representing air and ground. Taking measurements of electric and magnetic fields on a bounded subset of the surface of ground, henceforth called measurement device, corresponding to dipole excitations in the upper half space, we reconstruct the number and the positions of the unknown scatterers. Our assumption on the size of the scatterers is motivated by the fact that certain commercial metal detectors used for humanitarian demining work at comparatively low frequencies, i.e. with large wave lengths, while the mines itself (or the metal parts contained within the mines) are usually relatively small (cf., e.g., Bruschini [8] or Carruthers et al. [10]).

Since the seminal work of Devaney [17], MUSIC methods for reconstructing small or point-like scatterers from near of far field measurements of electromagnetic fields have been studied and implemented in two and three dimensions for homogeneous and inhomogeneous background media giving promising results.[1] See, e.g., Ammari et al. [1, 2, 3, 4], Cheney [11], Kirsch [27], Iakovleva et al. [24], and [21, 22, 23].

2000 *Mathematics Subject Classification.* Primary: 78A46, 35R30; Secondary: 35Q60, 35C20.
Key words and phrases. Inverse scattering, Maxwell's equations, small scatterers, reciprocity gap functional, layered media, asymptotic expansions.

[1] MUSIC is an acronym for MUltiple SIgnal Classification.

The theoretical foundation of these methods, which can be given along the lines developed by Brühl et al. [7], relies on an asymptotic analysis of the scattered fields on the measurement device as the size of the scatterers converges to zero. This analysis shows that these fields can be interpreted in the limit as fields generated by (fictitious) dipole sources located at the positions of the scatterers. Furthermore, one can conclude that a test point $\boldsymbol{y}$ in the lower half space coincides with one of these infinitesimally small scatterers, if and only if the field due to an artificial dipole source in $\boldsymbol{y}$, in the following called test dipole, evaluated on the measurement device belongs to the subspace spanned by the measured scattering data (cf. [21]).

For homogeneous background media MUSIC methods are known to be quite simple to implement and comparatively fast. However, this changes if the background medium is inhomogeneous, as, e.g., the two-layered medium considered here. Then the evaluation of the test dipole fields on the measurement device, which amounts to evaluating the Green's function for the background medium and has to be done for every test point in the search domain, is elaborate and slows down the algorithm significantly (cf. [22, 24]). Combining ideas from Reciprocity Gap Linear Sampling Methods developed by Colton et al. [13] (see also Cakoni et al. [9], and Monk et al. [29]) with the asymptotic analysis of the scattered field from [21], we establish the reciprocity gap MUSIC method (or RG-MUSIC method). This is a MUSIC reconstruction algorithm that requires data of the scattered and total electric and magnetic fields on the measurement device but avoids computing the Green's function for the background medium.

The article is organized as follows. After describing the basic modeling of our setting in the next section, we summarize the results of the asymptotic analysis from [21] in Section 3. In Section 4 we apply these results and study the asymptotic behavior of reciprocity gap functionals as considered in [9]. We proceed to develop the theoretical foundation of the RG-MUSIC method in Section 5 and derive a characterization of the positions of the scatterers in terms of the measured electromagnetic fields. In Section 6 we comment on the implementation of this characterization using the MUSIC approach, and in Section 7 we give numerical examples.

2. The mathematical setting.

We start with a mathematical description of our setting. Denote by $(\boldsymbol{e}_1, \boldsymbol{e}_2, \boldsymbol{e}_3)$ the usual Cartesian basis of $\mathbb{R}^3$, by $\boldsymbol{x} = (x_1, x_2, x_3)^\top$ and $\boldsymbol{y} = (y_1, y_2, y_3)^\top$ generic points in $\mathbb{R}^3$, and by $\boldsymbol{x} \cdot \boldsymbol{y}$ and $\boldsymbol{x} \times \boldsymbol{y}$ the scalar product and the vector product of $\boldsymbol{x}$ and $\boldsymbol{y}$, respectively.

Decomposing $\mathbb{R}^3$ in two half spaces $\mathbb{R}^3_+$ and $\mathbb{R}^3_-$ above and below the plane $\Sigma_0 := \{\boldsymbol{x} \in \mathbb{R}^3 \mid x_3 = 0\}$ representing the surface of ground we assume that both half spaces are filled with isotropic homogeneous materials modeling air and soil, respectively. The electric permittivity ε and the magnetic permeability μ of this two-layered medium are given by

$$\varepsilon(\boldsymbol{x}) := \begin{cases} \varepsilon_+, & \boldsymbol{x} \in \mathbb{R}^3_+, \\ \varepsilon_-, & \boldsymbol{x} \in \mathbb{R}^3_-, \end{cases} \qquad \mu(\boldsymbol{x}) := \begin{cases} \mu_+, & \boldsymbol{x} \in \mathbb{R}^3_+, \\ \mu_-, & \boldsymbol{x} \in \mathbb{R}^3_-, \end{cases}$$

with positive numbers ε_+, μ_+, and μ_-, whereas ε_- may be complex with positive real and nonnegative imaginary part to allow for conductive soils.

We investigate an inverse scattering problem for time-harmonic electromagnetic waves at a fixed frequency ω in presence of perfectly conducting small scatterers buried in the lower half space. These waves are supposed to be radiating solutions

of Maxwell's equations

$$\mathbf{curl}\boldsymbol{H} + \mathrm{i}\,\omega\varepsilon\boldsymbol{E} = \boldsymbol{0}, \quad \mathbf{curl}\boldsymbol{E} - \mathrm{i}\,\omega\mu\boldsymbol{H} = \boldsymbol{0} \tag{1}$$

outside some compact set $C \subset \mathbb{R}^3_-$. By this we understand (cf., e.g., Cutzach et al. [14] or Monk [28]) weak solutions in $\boldsymbol{H}_{\mathrm{loc}}(\mathbf{curl}, \mathbb{R}^3 \setminus \overline{C})$ which obey the Silver-Müller radiation condition

$$\int_{\partial B_r(\boldsymbol{0})} \left| \frac{\boldsymbol{x}}{r} \times \boldsymbol{H}(\boldsymbol{x}) + \left(\frac{\varepsilon(\boldsymbol{x})}{\mu(\boldsymbol{x})}\right)^{1/2} \boldsymbol{E}(\boldsymbol{x}) \right|^2 \mathrm{d}s(\boldsymbol{x}) = o(1) \qquad \text{as } r \to \infty,$$

where $B_r(\boldsymbol{0})$ denotes the ball of radius $r > 0$ around the origin. Note that $\boldsymbol{E}, \boldsymbol{H} \in \boldsymbol{H}_{\mathrm{loc}}(\mathbf{curl}, \mathbb{R}^3 \setminus \overline{C})$ implies that their tangential traces do not jump across the interface Σ_0. The associated discontinuous wave number is given by

$$k(\boldsymbol{x}) := \begin{cases} k_+ := \omega\sqrt{\varepsilon_+\mu_+}, & \boldsymbol{x} \in \mathbb{R}^3_+, \\ k_- := \omega\sqrt{\varepsilon_-\mu_-}, & \boldsymbol{x} \in \mathbb{R}^3_-, \end{cases}$$

with positive real and non-negative imaginary part.

Let $\mathcal{E} \subset \Sigma_d := \{\boldsymbol{x} \in \mathbb{R}^3 \mid x_3 = d\}$, $d > 0$, be a relatively open bounded domain in the upper half space. We consider incident waves $(\boldsymbol{E}^i(\,\cdot\,;\boldsymbol{x}_0,\boldsymbol{e}_j), \boldsymbol{H}^i(\,\cdot\,;\boldsymbol{x}_0,\boldsymbol{e}_j))$ generated by magnetic dipoles located at $\boldsymbol{x}_0 \in \mathcal{E}$ with horizontal polarizations $\boldsymbol{e}_j$, $j \in \{1,2\}$.[2] Introducing the magnetic dyadic Green's function $\mathbb{G}^m$ as the (distributional) solution of

$$\mathbf{curl}_x \frac{1}{\varepsilon(\boldsymbol{x})} \mathbf{curl}_x \mathbb{G}^m(\boldsymbol{x},\boldsymbol{y}) - \omega^2\mu(\boldsymbol{x})\mathbb{G}^m(\boldsymbol{x},\boldsymbol{y}) = \frac{1}{\varepsilon(\boldsymbol{x})}\delta(\boldsymbol{x}-\boldsymbol{y})\mathbb{I}_3, \tag{2}$$

$\boldsymbol{x}, \boldsymbol{y} \in \mathbb{R}^3$, where $\mathbb{I}_3$ denotes the 3×3 identity matrix, subject to the Silver-Müller radiation conditions

$$\int_{\partial B_r(\boldsymbol{0})} \left| \frac{\boldsymbol{x}}{r} \times \mathbb{G}^m(\boldsymbol{x},\boldsymbol{y}) + \frac{\mathrm{i}}{k(\boldsymbol{x})} \mathbf{curl}_x \mathbb{G}^m(\boldsymbol{x},\boldsymbol{y}) \right|^2 \mathrm{d}s(\boldsymbol{x}) = o(1),$$

$$\int_{\partial B_r(\boldsymbol{0})} \left| \frac{\boldsymbol{x}}{r} \times \mathbf{curl}_x \mathbb{G}^m(\boldsymbol{x},\boldsymbol{y}) + \mathrm{i}\,k(\boldsymbol{x}) \mathbb{G}^m(\boldsymbol{x},\boldsymbol{y}) \right|^2 \mathrm{d}s(\boldsymbol{x}) = o(1)$$

as $r \to \infty$, we can write these fields as

$$\boldsymbol{H}^i(\,\cdot\,;\boldsymbol{x}_0,\boldsymbol{e}_j) := k_+^2 \mathbb{G}^m(\,\cdot\,,\boldsymbol{x}_0)\boldsymbol{e}_j, \quad \boldsymbol{E}^i(\,\cdot\,;\boldsymbol{x}_0,\boldsymbol{e}_j) = -\frac{1}{\mathrm{i}\,\omega\varepsilon} \mathbf{curl}_x \boldsymbol{H}^i(\,\cdot\,;\boldsymbol{x}_0,\boldsymbol{e}_j). \tag{3}$$

For later reference we note that the electric dyadic Green's function $\mathbb{G}^e$ is defined analogously, but ε and μ have to be interchanged in (2).

We assume that a collection of perfectly conducting scatterers is buried in the lower half space $\mathbb{R}^3_-$, each of the form $D_{\delta,l} := \boldsymbol{z}_l + \delta B_l$, $1 \le l \le m$. Here $B_l \subset \mathbb{R}^3$ is a smoothly bounded open set containing the origin that consists of finitely many subdomains such that every subdomain is simply connected and its boundary is connected. We refer to the points $\boldsymbol{z}_l \in \mathbb{R}^3_-$ as the positions of the scatterers, to $0 < \delta \le 1$ as their size, and we assume that $|\boldsymbol{z}_j - \boldsymbol{z}_l| \ge c_0$ for $j \ne l$ and $\mathrm{dist}(\boldsymbol{z}_l, \Sigma_0) \ge c_0$ for some $c_0 > 0$, $1 \le j, l \le m$. The total collection of scatterers is denoted by $D_\delta := \bigcup_{l=1}^m (\boldsymbol{z}_l + \delta B_l)$.

Scattering of the incident field $(\boldsymbol{E}^i(\,\cdot\,;\boldsymbol{x}_0,\boldsymbol{e}_j), \boldsymbol{H}^i(\,\cdot\,;\boldsymbol{x}_0,\boldsymbol{e}_j))$ by these obstacles yields a scattered field $(\boldsymbol{E}^s(\,\cdot\,;\boldsymbol{x}_0,\boldsymbol{e}_j), \boldsymbol{H}^s(\,\cdot\,;\boldsymbol{x}_0,\boldsymbol{e}_j))$, which is a radiating solution of Maxwell's equations (1) in $\mathbb{R}^3 \setminus \overline{D_\delta}$ and fulfills the boundary condition

[2] Any other pair of linearly independent horizontal polarizations $(\boldsymbol{p}_1(\boldsymbol{x}_0), \boldsymbol{p}_2(\boldsymbol{x}_0))$ (not necessarily the same for all $\boldsymbol{x}_0 \in \mathcal{E}$) may be used instead of $(\boldsymbol{e}_1, \boldsymbol{e}_2)$ as well.

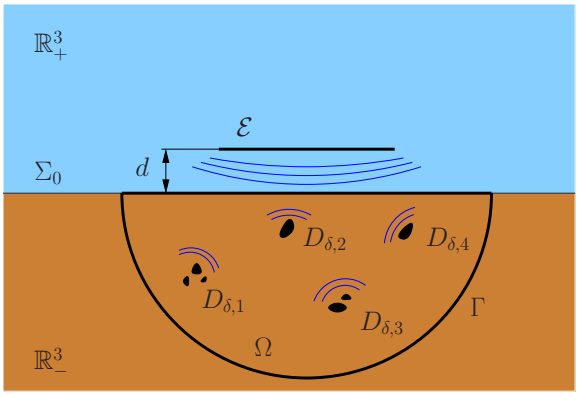

FIGURE 1. Sketch of the geometrical setup.

$\boldsymbol{\nu} \times \boldsymbol{E}^s(\,\cdot\,;\boldsymbol{x}_0,\boldsymbol{e}_j)|_{\partial D_\delta} = -\boldsymbol{\nu} \times \boldsymbol{E}^i(\,\cdot\,;\boldsymbol{x}_0,\boldsymbol{e}_j)|_{\partial D_\delta}$. The corresponding total electromagnetic field $(\boldsymbol{E}(\,\cdot\,;\boldsymbol{x}_0,\boldsymbol{e}_j), \boldsymbol{H}(\,\cdot\,;\boldsymbol{x}_0,\boldsymbol{e}_j))$ is the sum of the incident field and the scattered field.

Let $\Omega := B_R(\mathbf{0}) \cap \mathbb{R}^3_-$, $R > 0$, such that it contains all scatterers and denote its boundary by Γ (see Figure 1 for a sketch of the geometrical setup). In Section 3–6 we assume that the tangential traces $\boldsymbol{\nu} \times \boldsymbol{E}(\,\cdot\,;\boldsymbol{x}_0,\boldsymbol{e}_j)|_\Gamma$ and $\boldsymbol{\nu} \times \boldsymbol{H}(\,\cdot\,;\boldsymbol{x}_0,\boldsymbol{e}_j)|_\Gamma$ of the total field on Γ are known for any $\boldsymbol{x}_0 \in \mathcal{E}$ and any $j \in \{1,2\}$. We develop a method to reconstruct the positions of the scatterers from these data. Of course in practice it is not possible to measure all around the scatterers. However, choosing Ω large enough and taking into account the decay of the electromagnetic fields in the lower half space, we can restrict the measurements to $\Gamma \cap \Sigma_0$, i.e. to a bounded subset of the surface of ground, in the final implementation of the reconstruction algorithm, as we will exemplify by our numerical results.

3. The direct problem for small scatterers.

Throughout this work we assume that the scatterers are small with respect to the wavelength and with respect to their distance from each other and from the interface Σ_0. Under these assumptions the asymptotic behavior of the scattered field $(\boldsymbol{E}^s(\,\cdot\,;\boldsymbol{x}_0,\boldsymbol{e}_j), \boldsymbol{H}^s(\,\cdot\,;\boldsymbol{x}_0,\boldsymbol{e}_j))$ as the size of the scatterers δ tends to zero, i.e. as the scatterers $D_{\delta,l}$ shrink to the points $\boldsymbol{z}_l$, $l = 1,\dots,m$, has been studied in [21] and an asymptotic formula has been established (see also Ammari et al. [6] for a similar analysis for bounded domains). Although the incident fields considered in [21] are slightly different from (3), the results carry over to the present setup straightforwardly.

One building block of the asymptotic formula stated in Theorem 3.2 below are the magnetic and electric polarizability tensors for the domains $B_1,\dots,B_m$ (cf., e.g., Ammari and Kang [5] or Dassios and Kleinman [15]). For the readers convenience we recall their definition, which involves the transpose of the double layer operator ${K^0_{B_l}}^\top : H^{-1/2}(\partial B_l;\mathbb{C}) \to H^{-1/2}(\partial B_l;\mathbb{C})$,

$$\big({K^0_{B_l}}^\top \phi\big)(\boldsymbol{x}) := \int_{\partial B_l} \frac{\partial \Phi_0(\boldsymbol{x}-\boldsymbol{y})}{\partial \boldsymbol{\nu}(\boldsymbol{x})} \phi(\boldsymbol{y})\, \mathrm{d}s(\boldsymbol{y}), \qquad \boldsymbol{x} \in \partial B_l,$$

$l = 1,\dots,m$, where Φ_0 is the fundamental solution of the Laplace equation.

Definition 3.1. The magnetic and electric polarizability tensor $\mathbb{M}^0_{B_l} \in \mathbb{R}^{3\times 3}$ and $\mathbb{M}^\infty_{B_l} \in \mathbb{R}^{3\times 3}$ for the domain B_l, $l = 1, \dots, m$, is given by

$$\mathbb{M}^0_{B_l} := -\int_{\partial B_l} \boldsymbol{y}\left(\left(-\frac{1}{2}I + {K^0_{B_l}}^\top\right)^{-1}\boldsymbol{\nu}\right)^\top(\boldsymbol{y})\,\mathrm{d}s(\boldsymbol{y})$$

and

$$\mathbb{M}^\infty_{B_l} := \int_{\partial B_l} \boldsymbol{y}\left(\left(\frac{1}{2}I + {K^0_{B_l}}^\top\right)^{-1}\boldsymbol{\nu}\right)^\top(\boldsymbol{y})\,\mathrm{d}s(\boldsymbol{y}),$$

respectively.

It is well known that $\mathbb{M}^0_{B_l}$ and $\mathbb{M}^\infty_{B_l}$, $l = 1, \dots, m$, are symmetric and positive definite (cf., e.g., Friedman et al. [18] or [5, pp. 91–93]).

Theorem 3.2. ([21]) *For any source position $\boldsymbol{x}_0 \in \mathcal{E}$ and source polarization $\boldsymbol{e}_j$, $j \in \{1,2\}$, let $(\boldsymbol{E}^i(\,\cdot\,;\boldsymbol{x}_0,\boldsymbol{e}_j), \boldsymbol{H}^i(\,\cdot\,;\boldsymbol{x}_0,\boldsymbol{e}_j))$, be the incident field from (3), and denote by $\mathbb{M}^0_{B_1},\dots,\mathbb{M}^0_{B_m}$ and $\mathbb{M}^\infty_{B_1},\dots,\mathbb{M}^\infty_{B_m}$ the magnetic and electric polarizability tensors corresponding to $B_1,\dots,B_m$, respectively. Then,*

$$\begin{aligned}
&\boldsymbol{\nu}\times\boldsymbol{H}^s(\,\cdot\,;\boldsymbol{x}_0,\boldsymbol{e}_j)\big|_\Gamma \\
&\qquad = \delta^3\sum_{l=1}^m\Big(-k_-^2\,\boldsymbol{\nu}\times\mathbb{G}^m(\,\cdot\,,\boldsymbol{z}_l)\big|_\Gamma\mathbb{M}^0_{B_l}\boldsymbol{H}^i(\boldsymbol{z}_l;\boldsymbol{x}_0,\boldsymbol{e}_j) \\
&\qquad\quad + \frac{\mu_-}{\mu_+}\boldsymbol{\nu}\times\mathbf{curl}_x\mathbb{G}^e(\,\cdot\,,\boldsymbol{z}_l)\big|_\Gamma\mathbb{M}^\infty_{B_l}\mathbf{curl}\boldsymbol{H}^i(\boldsymbol{z}_l;\boldsymbol{x}_0,\boldsymbol{e}_j)\Big) + \mathcal{O}(\delta^4),
\end{aligned} \tag{4}$$

$$\begin{aligned}
&\boldsymbol{\nu}\times\mathbf{curl}\boldsymbol{H}^s(\,\cdot\,;\boldsymbol{x}_0,\boldsymbol{e}_j)\big|_\Gamma \\
&\qquad = \delta^3\sum_{l=1}^m\Big(-k_-^2\,\boldsymbol{\nu}\times\mathbf{curl}_x\mathbb{G}^m(\,\cdot\,,\boldsymbol{z}_l)\big|_\Gamma\mathbb{M}^0_{B_l}\boldsymbol{H}^i(\boldsymbol{z}_l;\boldsymbol{x}_0,\boldsymbol{e}_j) \\
&\qquad\quad + k_-^2\,\frac{\mu_-}{\mu_+}\boldsymbol{\nu}\times\mathbb{G}^e(\,\cdot\,,\boldsymbol{z}_l)\big|_\Gamma\mathbb{M}^\infty_{B_l}\mathbf{curl}\boldsymbol{H}^i(\boldsymbol{z}_l;\boldsymbol{x}_0,\boldsymbol{e}_j)\Big) + \mathcal{O}(\delta^4)
\end{aligned} \tag{5}$$

in $\boldsymbol{H}^{-1/2}_{\mathrm{div}}(\Gamma)$ as $\delta\to 0$. The terms $\mathcal{O}(\delta^4)$ are bounded by $C\delta^4$, uniformly for $\boldsymbol{x}_0\in\mathcal{E}$, and the constant C is independent of δ.

4. **The reciprocity gap functional.** Let $\mathcal{D}'(\Omega;\mathbb{C}^3)$ denote the space of distributions on Ω with values in $\mathbb{C}^3$ and define the (locally convex) vector space

$$\boldsymbol{W}(\Omega) := \left\{\boldsymbol{u}\in\mathcal{D}'(\Omega;\mathbb{C}^3)\mid \exists C\subset\subset\Omega\,:\,\boldsymbol{u},\mathbf{curl}\boldsymbol{u}\in\boldsymbol{H}(\mathbf{curl},\Omega\setminus\overline{C})\right\}.$$

We follow [9] and introduce the reciprocity gap functional $R:\boldsymbol{W}(\Omega)\times\boldsymbol{W}(\Omega)\to\mathbb{C}$,

$$R(\boldsymbol{u},\boldsymbol{v}) := \int_\Gamma(\boldsymbol{\nu}\times\boldsymbol{u}\cdot\mathbf{curl}\boldsymbol{v} - \boldsymbol{\nu}\times\boldsymbol{v}\cdot\mathbf{curl}\boldsymbol{u})\,\mathrm{d}\boldsymbol{x}. \tag{6}$$

By Green's formula (cf. [28, Thm. 3.31]) $R(\boldsymbol{u},\boldsymbol{v}) = 0$, if $\boldsymbol{u}$ and $\boldsymbol{v}$ are (distributional) solutions of

$$\mathbf{curlcurl}\boldsymbol{w} - k_-^2\,\boldsymbol{w} = \boldsymbol{0} \tag{7}$$

in Ω. Substituting $\boldsymbol{u} := \boldsymbol{H}(\,\cdot\,;\boldsymbol{x}_0,\boldsymbol{e}_j)|_\Omega$ for $\boldsymbol{x}_0\in\mathcal{E}$ and $j\in\{1,2\}$ in (6) we obtain the reciprocity gap operator $F_\delta:\boldsymbol{W}(\Omega)\to L^2_t(\mathcal{E};\mathbb{C}^3)$,

$$(F_\delta\boldsymbol{v})(\boldsymbol{x}_0) := \big(R(\boldsymbol{H}(\,\cdot\,;\boldsymbol{x}_0,\boldsymbol{e}_1),\boldsymbol{v}), R(\boldsymbol{H}(\,\cdot\,;\boldsymbol{x}_0,\boldsymbol{e}_2),\boldsymbol{v}), 0\big)^\top,$$

where

$$L_t^2(\mathcal{E};\mathbb{C}^3) := \left\{ \boldsymbol{a} \in L^2(\mathcal{E};\mathbb{C}^3) \mid \boldsymbol{e}_3 \cdot \boldsymbol{a} = 0 \right\}.$$

Here the subscript δ indicates that F_δ depends on the size δ of the scatterers D_δ.

Next we recall the dyadic Green's function $\mathbb{G}_{k_-}$ for Maxwell's equations in a homogeneous medium with constant wave number k_-,

$$\mathbb{G}_{k_-}(\boldsymbol{x},\boldsymbol{y}) := \Phi_{k_-}(\boldsymbol{x},\boldsymbol{y})\mathbb{I}_3 + \frac{1}{k_-^2}\nabla_x \operatorname{div}_x\big(\Phi_{k_-}(\boldsymbol{x},\boldsymbol{y})\mathbb{I}_3\big), \quad \boldsymbol{x},\boldsymbol{y} \in \mathbb{R}^3, \boldsymbol{x} \neq \boldsymbol{y},$$

where Φ_{k_-} denotes the fundamental solution of the Helmholtz equation. The matrix-valued function $\mathbb{G}_{k_-}(\,\cdot\,,\boldsymbol{y})$ solves (7) in $\mathbb{R}^3 \setminus \{\boldsymbol{y}\}$. Accordingly, the single layer operator $S_\mathcal{E} : L_t^2(\mathcal{E};\mathbb{C}^3) \to \boldsymbol{H}_{\mathrm{loc}}(\mathbf{curl},\mathbb{R}^3 \setminus \mathcal{E})$,

$$S_\mathcal{E}\boldsymbol{\phi} := \int_\mathcal{E} \mathbb{G}_{k_-}(\,\cdot\,,\boldsymbol{y})\boldsymbol{\phi}(\boldsymbol{y})\, \mathrm{d}s(\boldsymbol{y}),$$

yields solutions of (7) in Ω.

To develop our reconstruction method we study the equation

$$F_\delta(S_\mathcal{E}\boldsymbol{\phi}) = F_\delta(\mathbb{G}_{k_-}(\,\cdot\,,\boldsymbol{y})\boldsymbol{d}) \tag{8}$$

for $\boldsymbol{y} \in \Omega$ and $\boldsymbol{d} \in \mathbb{C}^3 \setminus \{\boldsymbol{0}\}$. This equation is also the foundation of the Reciprocity Gap Linear Sampling Method proposed in [9]. Defining the operator

$$A_\delta := F_\delta \circ S_\mathcal{E} : L_t^2(\mathcal{E};\mathbb{C}^3) \to L_t^2(\mathcal{E};\mathbb{C}^3), \tag{9}$$

we find by interchanging the order of integration that

$$(A_\delta\boldsymbol{\phi})_j(\boldsymbol{x}_0) = \int_\mathcal{E} R\big(\boldsymbol{H}(\,\cdot\,;\boldsymbol{x}_0,\boldsymbol{e}_j), \mathbb{G}_{k_-}(\,\cdot\,,\boldsymbol{y})\big)\boldsymbol{\phi}(\boldsymbol{y})\, \mathrm{d}s(\boldsymbol{y})$$

for $j \in \{1,2\}$. So (8) can be written as

$$A_\delta\boldsymbol{\phi} = F_\delta(\mathbb{G}_{k_-}(\,\cdot\,,\boldsymbol{y})\boldsymbol{d}), \tag{10}$$

which is an integral equation of the first kind that is ill-posed since A_δ is compact.

We are interested in the asymptotic behavior of A_δ as $\delta \to 0$. Since for all $\boldsymbol{x}_0 \in \mathcal{E}$ and $j \in \{1,2\}$ the incident magnetic field $\boldsymbol{H}^i(\,\cdot\,;\boldsymbol{x}_0,\boldsymbol{e}_j)$ is a solution of (7) in Ω, we find from Green's formula that $R(\boldsymbol{H}^i(\,\cdot\,;\boldsymbol{x}_0,\boldsymbol{e}_j), S_\mathcal{E}\boldsymbol{\phi}) = 0$ and thus

$$(A_\delta\boldsymbol{\phi})_j(\boldsymbol{x}_0) = R(\boldsymbol{H}^s(\,\cdot\,;\boldsymbol{x}_0,\boldsymbol{e}_j), S_\mathcal{E}\boldsymbol{\phi}). \tag{11}$$

Using the asymptotic expansions (4) and (5) we obtain that

$$\begin{aligned}
&R(\boldsymbol{H}^s(\,\cdot\,;\boldsymbol{x}_0,\boldsymbol{e}_j), S_\mathcal{E}\boldsymbol{\phi}) \\
&\quad= R\Big(\delta^3 \sum_{l=1}^m \Big(-k_-^2\,\mathbb{G}^m(\,\cdot\,,\boldsymbol{z}_l)\mathbb{M}_{B_l}^0\boldsymbol{H}^i(\boldsymbol{z}_l;\boldsymbol{x}_0,\boldsymbol{e}_j) \\
&\qquad + \frac{\mu_-}{\mu_+}\mathbf{curl}_x\mathbb{G}^e(\,\cdot\,,\boldsymbol{z}_l)\mathbb{M}_{B_l}^\infty\mathbf{curl}\boldsymbol{H}^i(\boldsymbol{z}_l;\boldsymbol{x}_0,\boldsymbol{e}_j)\Big) + \mathcal{O}(\delta^4), S_\mathcal{E}\boldsymbol{\phi}\Big) \\
&\quad= \delta^3 \sum_{l=1}^m \Big(-k_-^2\,R\big(\mathbb{G}^m(\,\cdot\,,\boldsymbol{z}_l), S_\mathcal{E}\boldsymbol{\phi}\big)\mathbb{M}_{B_l}^0\boldsymbol{H}^i(\boldsymbol{z}_l;\boldsymbol{x}_0,\boldsymbol{e}_j) \\
&\qquad + \frac{\mu_-}{\mu_+}R\big(\mathbf{curl}_x\mathbb{G}^e(\,\cdot\,,\boldsymbol{z}_l), S_\mathcal{E}\boldsymbol{\phi}\big)\mathbb{M}_{B_l}^\infty\mathbf{curl}\boldsymbol{H}^i(\boldsymbol{z}_l;\boldsymbol{x}_0,\boldsymbol{e}_j)\Big) + \mathcal{O}(\delta^4).
\end{aligned}$$

The Stratton-Chu formula (cf. [28, Thm. 9.2]) yields for $l = 1, \dots, m$ that

$$\begin{aligned} R\big(\mathbb{G}^m(\,\cdot\,, \boldsymbol{z}_l), S_{\mathcal{E}}\boldsymbol{\phi}\big) &= -\int_\Gamma \Big((\boldsymbol{\nu} \times \mathbf{curl} S_{\mathcal{E}}\boldsymbol{\phi})^\top(\boldsymbol{x}) \mathbb{G}^m(\boldsymbol{x}, \boldsymbol{z}_l) \\ &\qquad + (\boldsymbol{\nu} \times S_{\mathcal{E}}\boldsymbol{\phi})^\top(\boldsymbol{x}) \mathbf{curl}_x \mathbb{G}^m(\boldsymbol{x}, \boldsymbol{z}_l) \Big)\, ds(\boldsymbol{x}) \\ &= (S_{\mathcal{E}}\boldsymbol{\phi})^\top(\boldsymbol{z}_l). \end{aligned}$$

Similarly, using integration by parts and Maxwell's equations we obtain that

$$\begin{aligned} R\big(\mathbf{curl}_x \mathbb{G}^e(\,\cdot\,, \boldsymbol{z}_l), S_{\mathcal{E}}\boldsymbol{\phi}\big) &= -\int_\Gamma \Big((\boldsymbol{\nu} \times \mathbf{curl} S_{\mathcal{E}}\boldsymbol{\phi})^\top(\boldsymbol{x}) \mathbf{curl}_x \mathbb{G}^e(\boldsymbol{x}, \boldsymbol{z}_l) \\ &\qquad + (\boldsymbol{\nu} \times S_{\mathcal{E}}\boldsymbol{\phi})^\top(\boldsymbol{x}) \mathbf{curlcurl} \mathbb{G}^e(\boldsymbol{x}, \boldsymbol{z}_l) \Big)\, ds(\boldsymbol{x}) \\ &= -\int_\Gamma \Big((\boldsymbol{\nu} \times \mathbf{curlcurl} S_{\mathcal{E}}\boldsymbol{\phi})^\top(\boldsymbol{x}) \mathbb{G}^e(\boldsymbol{x}, \boldsymbol{z}_l) \\ &\qquad + (\boldsymbol{\nu} \times \mathbf{curl} S_{\mathcal{E}}\boldsymbol{\phi})^\top(\boldsymbol{x}) \mathbf{curl}_x \mathbb{G}^e(\boldsymbol{x}, \boldsymbol{z}_l) \Big)\, ds(\boldsymbol{x}) \\ &= (\mathbf{curl} S_{\mathcal{E}}\boldsymbol{\phi})^\top(\boldsymbol{z}_l). \end{aligned}$$

Thus, recalling the definition of the incident magnetic field $\boldsymbol{H}^i(\,\cdot\,; \boldsymbol{x}_0, \boldsymbol{e}_j)$ from (3),

$$\begin{aligned} (A_\delta \boldsymbol{\phi})_j = \delta^3 \sum_{l=1}^m \Big(& -k_+^2 k_-^2 (S_{\mathcal{E}}\boldsymbol{\phi})^\top(\boldsymbol{z}_l) \mathbb{M}^0_{B_l} \mathbb{G}^m(\boldsymbol{z}_l, \,\cdot\,) \boldsymbol{e}_j \\ & + k_+^2 \frac{\mu_-}{\mu_+} (\mathbf{curl} S_{\mathcal{E}}\boldsymbol{\phi})^\top(\boldsymbol{z}_l) \mathbb{M}^\infty_{B_l} \mathbf{curl}_x \mathbb{G}^m(\boldsymbol{z}_l, \,\cdot\,) \boldsymbol{e}_j \Big) + \mathcal{O}(\delta^4). \end{aligned} \tag{12}$$

Next we study the asymptotic behavior of the right hand side of (10). For $\boldsymbol{x}_0 \in \mathcal{E}$ and $j \in \{1, 2\}$,

$$\begin{aligned} &\big(\big(F_\delta(\mathbb{G}_{k_-}(\,\cdot\,, \boldsymbol{y})\boldsymbol{d})(x_0) \big) \big)_j = R\big(\boldsymbol{H}(\,\cdot\,; \boldsymbol{x}_0, \boldsymbol{e}_j), \mathbb{G}_{k_-}(\,\cdot\,, \boldsymbol{y})\boldsymbol{d}\big) \\ &= R\big(k_+^2 \mathbb{G}^m(\,\cdot\,, \boldsymbol{x}_0)\boldsymbol{e}_j, \mathbb{G}_{k_-}(\,\cdot\,, \boldsymbol{y})\boldsymbol{d}\big) \\ &\quad + R\Big(\delta^3 \sum_{l=1}^m \Big(-k_-^2 \mathbb{G}^m(\,\cdot\,, \boldsymbol{z}_l) \mathbb{M}^0_{B_l} \boldsymbol{H}^i(\boldsymbol{z}_l; \boldsymbol{x}_0, \boldsymbol{e}_j) \\ &\qquad + \frac{\mu_-}{\mu_+} \mathbf{curl}_x \mathbb{G}^e(\,\cdot\,, \boldsymbol{z}_l) \mathbb{M}^\infty_{B_l} \mathbf{curl} \boldsymbol{H}^i(\boldsymbol{z}_l; \boldsymbol{x}_0, \boldsymbol{e}_j) \Big) + \mathcal{O}(\delta^4), \mathbb{G}_{k_-}(\,\cdot\,, \boldsymbol{y})\boldsymbol{d} \Big). \end{aligned}$$

Applying the Stratton-Chu formula and the reciprocity relation

$$\varepsilon(\boldsymbol{y}) \mathbb{G}^m(\boldsymbol{x}, \boldsymbol{y}) = \varepsilon(\boldsymbol{x}) (\mathbb{G}^m(\boldsymbol{y}, \boldsymbol{x}))^\top, \qquad \boldsymbol{x}, \boldsymbol{y} \in \mathbb{R}^3 \setminus \Sigma_0,\ \boldsymbol{x} \neq \boldsymbol{y}, \tag{13}$$

(cf. Chew [12, p. 411] or [20, p. 122]) we obtain for the first part that

$$\begin{aligned} &R\big(k_+^2 \mathbb{G}^m(\,\cdot\,, \boldsymbol{x}_0)\boldsymbol{e}_j, \mathbb{G}_{k_-}(\,\cdot\,, \boldsymbol{y})\boldsymbol{d}\big) \\ &\qquad = k_+^2 \int_\Gamma \boldsymbol{e}_j^\top \Big(\big(\boldsymbol{\nu}(\boldsymbol{x}) \times \mathbb{G}^m(\boldsymbol{x}, \boldsymbol{x}_0) \big)^\top \mathbf{curl}_x \mathbb{G}_{k_-}(\boldsymbol{x}, \boldsymbol{y}) \\ &\qquad\qquad + \big(\boldsymbol{\nu}(\boldsymbol{x}) \times \mathbf{curl} \mathbb{G}^m(\boldsymbol{x}, \boldsymbol{x}_0) \big)^\top \mathbb{G}_{k_-}(\boldsymbol{x}, \boldsymbol{y}) \Big) \boldsymbol{d}\, ds(\boldsymbol{x}) \\ &\qquad = -k_+^2 \boldsymbol{e}_j^\top \big(\mathbb{G}^m(\boldsymbol{y}, \boldsymbol{x}_0) \big)^\top \boldsymbol{d} = -k_+^2 \frac{\varepsilon_-}{\varepsilon_+} \boldsymbol{e}_j^\top \mathbb{G}^m(\boldsymbol{x}_0, \boldsymbol{y}) \boldsymbol{d}. \end{aligned}$$

Furthermore, using (13) and the formula

$$k^2(\boldsymbol{y})\mathbf{curl}_x\mathbb{G}^e(\boldsymbol{x},\boldsymbol{y}) = k^2(\boldsymbol{x})\big(\mathbf{curl}_y\mathbb{G}^m(\boldsymbol{y},\boldsymbol{x})\big)^\top, \qquad \boldsymbol{x},\boldsymbol{y}\in\mathbb{R}^3\setminus\Sigma_0,\ \boldsymbol{x}\neq\boldsymbol{y}, \tag{14}$$

(cf. [24] or [20, p. 124]), the second part can be written as

$$\delta^3\sum_{l=1}^m\Big(-k_+^2k_-^2\frac{\varepsilon_-}{\varepsilon_+}\boldsymbol{e}_j^\top\mathbb{G}^m(\boldsymbol{x}_0,\boldsymbol{z}_l)\mathbb{M}^0_{B_l}R\big(\mathbb{G}^m(\,\cdot\,,\boldsymbol{z}_l),\mathbb{G}_{k_-}(\,\cdot\,,\boldsymbol{y})\boldsymbol{d}\big)$$
$$+k_-^2\frac{\mu_-}{\mu_+}\boldsymbol{e}_j^\top\mathbf{curl}_x\mathbb{G}^e(\boldsymbol{x}_0,\boldsymbol{z}_l)\mathbb{M}^\infty_{B_l}R\big(\mathbf{curl}_x\mathbb{G}^e(\,\cdot\,,\boldsymbol{z}_l),\mathbb{G}_{k_-}(\,\cdot\,,\boldsymbol{y})\boldsymbol{d}\big)\Big)+\mathcal{O}(\delta^4).$$

In sum,

$$F_\delta\big(\mathbb{G}_{k_-}(\,\cdot\,,\boldsymbol{y})\boldsymbol{d}\big) = -k_+^2\frac{\varepsilon_-}{\varepsilon_+}\big(\boldsymbol{e}_3\times\mathbb{G}^m(\,\cdot\,,\boldsymbol{y})\boldsymbol{d}\big)\times\boldsymbol{e}_3+\mathcal{O}(\delta^3), \tag{15}$$

in $L^2_t(\mathcal{E};\mathbb{C}^3)$ and the term $\mathcal{O}(\delta^3)$ is smooth away from $\boldsymbol{z}_1,\dots,\boldsymbol{z}_m$.

Remark 1. These calculations also imply that

$$R\big(\boldsymbol{H}^i(\,\cdot\,;\boldsymbol{x}_0,\boldsymbol{e}_j),\mathbb{G}_{k_-}(\,\cdot\,,\boldsymbol{y})\boldsymbol{d}\big) = -k_+^2\frac{\varepsilon_-}{\varepsilon_+}\boldsymbol{e}_j^\top\mathbb{G}^m(\boldsymbol{x}_0,\boldsymbol{y})\boldsymbol{d} \tag{16}$$

for $\boldsymbol{x}_0\in\mathcal{E}$ and $j\in\{1,2\}$.

5. **The characterization of the scatterers.** In the following we use the asymptotic expansion of $A_\delta\boldsymbol{\phi}$ in (12) and the expansion of $F_\delta(\mathbb{G}_{k_-}(\,\cdot\,,\boldsymbol{y})\boldsymbol{d})$ in (15) to characterize the positions of the scatterers $\boldsymbol{z}_1,\dots,\boldsymbol{z}_m$. To that end we consider the leading order term in (12) and define the operator $T: L^2_t(\mathcal{E};\mathbb{C}^3)\to L^2_t(\mathcal{E};\mathbb{C}^3)$,

$$(T\boldsymbol{\phi})_j := \sum_{l=1}^m\Big(-k_+^2k_-^2(S_\mathcal{E}\boldsymbol{\phi})^\top(\boldsymbol{z}_l)\mathbb{M}^0_{B_l}\mathbb{G}^m(\boldsymbol{z}_l,\cdot)\boldsymbol{e}_j$$
$$+k_+^2\frac{\mu_-}{\mu_+}(\mathbf{curl}S_\mathcal{E}\boldsymbol{\phi})^\top(\boldsymbol{z}_l)\mathbb{M}^\infty_{B_l}\mathbf{curl}_x\mathbb{G}^m(\boldsymbol{z}_l,\cdot)\boldsymbol{e}_j\Big), \qquad j=1,2,$$

and $(T\boldsymbol{\phi})_3=0$. Applying the reciprocity relations (13) and (14) and the symmetry of the polarizability tensors, we find that

$$T\boldsymbol{\phi} = \sum_{l=1}^m\Big(\boldsymbol{e}_3\times\Big(-k_+^2k_-^2\frac{\varepsilon_-}{\varepsilon_+}\mathbb{G}^m(\,\cdot\,,\boldsymbol{z}_l)\mathbb{M}^0_{B_l}(S_\mathcal{E}\boldsymbol{\phi})(\boldsymbol{z}_l)$$
$$+k_-^2\frac{\mu_-}{\mu_+}\mathbf{curl}_x\mathbb{G}^e(\,\cdot\,,\boldsymbol{z}_l)\mathbb{M}^\infty_{B_l}(\mathbf{curl}S_\mathcal{E}\boldsymbol{\phi})(\boldsymbol{z}_l)\Big)\Big)\times\boldsymbol{e}_3.$$

The operator T is linear and fulfills

$$A_\delta = \delta^3T+\mathcal{O}(\delta^4) \tag{17}$$

as $\delta\to0$ in $\mathcal{L}(L^2_t(\mathcal{E};\mathbb{C}^3),L^2_t(\mathcal{E};\mathbb{C}^3))$, i.e. in the space of bounded linear operators form $L^2_t(\mathcal{E};\mathbb{C}^3)$ into itself. It admits a factorization $T=RMS$, where $S: L^2_t(\mathcal{E};\mathbb{C}^3)\to\mathbb{C}^{3\times2m}$ is given by

$$S\boldsymbol{\phi} := \big((S_\mathcal{E}\boldsymbol{\phi})(\boldsymbol{z}_1),\dots,(S_\mathcal{E}\boldsymbol{\phi})(\boldsymbol{z}_m),(\mathbf{curl}S_\mathcal{E}\boldsymbol{\phi})(\boldsymbol{z}_1),\dots,(\mathbf{curl}S_\mathcal{E}\boldsymbol{\phi})(\boldsymbol{z}_m)\big),$$

$M:\mathbb{C}^{3\times2m}\to\mathbb{C}^{3\times2m}$ is defined by

$$M\boldsymbol{a} := \Big(-k_-^2k_+^2\frac{\varepsilon_-}{\varepsilon_+}\mathbb{M}^0_{B_1}\boldsymbol{a}_1,\dots,-k_-^2k_+^2\frac{\varepsilon_-}{\varepsilon_+}\mathbb{M}^0_{B_m}\boldsymbol{a}_m,$$
$$k_-^2\frac{\mu_-}{\mu_+}\mathbb{M}^\infty_{B_1}\boldsymbol{a}_{m+1},\dots,k_-^2\frac{\mu_-}{\mu_+}\mathbb{M}^\infty_{B_m}\boldsymbol{a}_{2m}\Big),$$

and $R : \mathbb{C}^{3\times 2m} \to L_t^2(\mathcal{E};\mathbb{C}^3)$ is given by

$$R\boldsymbol{a} := \sum_{l=1}^{m} \Big(\boldsymbol{e}_3 \times \Big(\mathbb{G}^m(\,\cdot\,,\boldsymbol{z}_l)\boldsymbol{a}_l + \mathbf{curl}_x \mathbb{G}^e(\,\cdot\,,\boldsymbol{z}_l)\boldsymbol{a}_{m+l} \Big) \Big) \times \boldsymbol{e}_3.$$

Lemma 5.1. *(a) R is injective. (b) S is surjective. (c) M is bijective.*

Proof. Part (a) can be proved similarly to Lemma 9.1 from [21]. In the following we sketch the main steps of the proof and refer the reader to [21] for details. Suppose $\boldsymbol{a} \in \mathbb{C}^{3\times 2m}$ is in the nullspace of R. Then,

$$\boldsymbol{H}^a := \sum_{l=1}^{m} \big(\mathbb{G}^m(\,\cdot\,,\boldsymbol{z}_l)\boldsymbol{a}_l + \mathbf{curl}_x \mathbb{G}^e(\,\cdot\,,\boldsymbol{z}_l)\boldsymbol{a}_{m+l} \big)$$

together with the associated electric field $\boldsymbol{E}^a := -1/(\mathrm{i}\omega\varepsilon)\mathbf{curl}\boldsymbol{H}^a$ is a radiating solution of Maxwell's equations (1) in $\mathbb{R}^3 \setminus \bigcup_{l=1}^m \{\boldsymbol{z}_l\}$ that satisfies $(\boldsymbol{e}_3 \times \boldsymbol{H}^a|_{\mathcal{E}}) \times \boldsymbol{e}_3 = \boldsymbol{0}$. Applying analytic continuation, a reflection argument, and Holmgren's Theorem it follows that $\boldsymbol{H}^a = \boldsymbol{0}$ in $\mathbb{R}^3 \setminus \bigcup_{l=1}^m \{\boldsymbol{z}_l\}$. If $\boldsymbol{a}_l \neq \boldsymbol{0}$ for some $l \in \{1,\dots,m\}$, the singularities of $\mathbb{G}^m(\boldsymbol{x},\boldsymbol{z}_l)$ and $\mathbf{curl}_x \mathbb{G}^m(\boldsymbol{x},\boldsymbol{z}_l)$ at $\boldsymbol{z}_l$ imply that $|\boldsymbol{H}^a(\boldsymbol{x})|$ becomes unbounded as $\boldsymbol{x}$ approaches $\boldsymbol{z}_l$. This is a contradiction and thus $\boldsymbol{a} = \boldsymbol{0}$.

Observing that the transpose $S^\top : \mathbb{C}^{3\times 2m} \to L_t^2(\mathcal{E};\mathbb{C}^3)$ of S is given by

$$S^\top \boldsymbol{a} = \sum_{l=1}^{m} \Big(\boldsymbol{e}_3 \times \Big(\mathbb{G}_{k_-}(\,\cdot\,,\boldsymbol{z}_l)\boldsymbol{a}_l + \mathbf{curl}_x \mathbb{G}_{k_-}(\,\cdot\,,\boldsymbol{z}_l)\boldsymbol{a}_{m+l} \Big) \Big) \times \boldsymbol{e}_3,$$

we find as in part (a) that $S^\top$ is injective. Since $\mathcal{R}(S)$ is finite dimensional, we obtain that $\mathcal{R}(S) = \mathcal{N}(S^\top)^a = \mathbb{C}^{3\times 2m}$, which proves part (b). Here $\mathcal{N}(S^\top)^a$ denotes the annihilator of $\mathcal{N}(S^\top)$ in $\mathbb{C}^{3\times 2m}$.

Part (c) follows directly from the positive definiteness of the polarizability tensors. □

Proposition 1. *The range of T has dimension $6m$ and is given by*

$$\mathcal{R}(T) = \mathrm{span}_{\mathbb{C}} \big\{ \big(\boldsymbol{e}_3 \times (\mathbb{G}^m(\,\cdot\,,\boldsymbol{z}_l)\boldsymbol{e}_j) \big) \times \boldsymbol{e}_3 \,, \\ \big(\boldsymbol{e}_3 \times (\mathbf{curl}_x \mathbb{G}^e(\,\cdot\,,\boldsymbol{z}_l)\boldsymbol{e}_j) \big) \times \boldsymbol{e}_3 \;\big|\; j = 1,2,3;\ l = 1,\dots,m \big\}.$$

Proof. The surjectivity of S and M implies that $\mathcal{R}(T) = \mathcal{R}(RMS) = \mathcal{R}(R)$. So, the proposition follows from the definition of R and its injectivity. □

Using Proposition 1 we can show the following characterization of the positions of the scatterers $\boldsymbol{z}_1,\dots,\boldsymbol{z}_m$.

Proposition 2. *Let $\boldsymbol{d} \in \mathbb{C}^3 \setminus \{\boldsymbol{0}\}$, $\boldsymbol{y} \in \Omega$, and*

$$\boldsymbol{g}_{y,d} := \big(\boldsymbol{e}_3 \times (\mathbb{G}^m(\,\cdot\,,\boldsymbol{y})\boldsymbol{d}) \times \boldsymbol{e}_3 \big)\big|_{\mathcal{E}}\,. \tag{18}$$

Then, $\boldsymbol{g}_{y,d} \in \mathcal{R}(T)$ if and only if $\boldsymbol{y} \in \{\boldsymbol{z}_1,\dots,\boldsymbol{z}_m\}$.

Proof. This proof is similar to the proof of [21, Prop. 9.2]. Assuming that $\boldsymbol{g}_{y,d} \in \mathcal{R}(T)$, we find from Proposition 1 that $\boldsymbol{g}_{y,d}$ can be written as

$$\boldsymbol{g}_{y,d} = \sum_{l=1}^{m} \Big(\boldsymbol{e}_3 \times \big(\mathbb{G}^m(\,\cdot\,,\boldsymbol{z}_l)\boldsymbol{a}_l + \mathbf{curl}_x \mathbb{G}^e(\,\cdot\,,\boldsymbol{z}_l)\boldsymbol{a}_{l+m} \big) \Big) \times \boldsymbol{e}_3 \qquad \text{on } \mathcal{E},$$

with $\boldsymbol{a}_1, \dots, \boldsymbol{a}_{2m} \in \mathbb{C}^3$. But then both,

$$\boldsymbol{H}^a := \sum_{l=1}^{m} \Big(\mathbb{G}^m(\,\cdot\,, \boldsymbol{z}_l)\boldsymbol{a}_l + \mathbf{curl}_x \mathbb{G}^e(\,\cdot\,, \boldsymbol{z}_l)\boldsymbol{a}_{l+m} \Big) \quad \text{and} \quad \boldsymbol{H}^d := \mathbb{G}^m(\,\cdot\,, \boldsymbol{y})\boldsymbol{d}$$

together with the corresponding electric fields are radiating solutions of Maxwell's equations (1) in $\mathbb{R}^3 \setminus (\bigcup_{l=1}^m \{\boldsymbol{z}_l\} \cup \{\boldsymbol{y}\})$ and their tangential components coincide on $\mathcal{E}$. Hence, $\tilde{\boldsymbol{H}} := \boldsymbol{H}^a - \boldsymbol{H}^d$ together with the associated electric field $\tilde{\boldsymbol{E}}$ is a radiating solution of (1) in $\mathbb{R}^3 \setminus (\bigcup_{l=1}^m \{\boldsymbol{z}_l\} \cup \{\boldsymbol{y}\})$ that satisfies $(\boldsymbol{e}_3 \times \tilde{\boldsymbol{H}}|_{\mathcal{E}}) \times \boldsymbol{e}_3 = \mathbf{0}$. Now we conclude as in the proof of Lemma 5.1 that $(\tilde{\boldsymbol{E}}, \tilde{\boldsymbol{H}})$ vanishes everywhere in $\mathbb{R}^3 \setminus (\bigcup_{l=1}^m \{\boldsymbol{z}_l\} \cup \{\boldsymbol{y}\})$. Thus, $\boldsymbol{H}^a = \boldsymbol{H}^d$ in $\mathbb{R}^3 \setminus (\bigcup_{l=1}^m \{\boldsymbol{z}_l\} \cup \{\boldsymbol{y}\})$. This is only possible if $\boldsymbol{y} \in \{\boldsymbol{z}_1, \dots, \boldsymbol{z}_m\}$, which shows the necessity of this condition. Its sufficiency follows directly from Proposition 1. □

6. **The reciprocity gap MUSIC method.** To find the positions of the scatterers $\boldsymbol{z}_1, \dots, \boldsymbol{z}_m$ we place a grid of test points in the region where the scatterers are supposed to be, i.e. in the search domain. Then the idea is to check for each test point $\boldsymbol{y}$ on this grid and some fixed $\boldsymbol{d} \in \mathbb{C}^3 \setminus \{\mathbf{0}\}$ whether the test function $\boldsymbol{g}_{y,d}$ from (18) belongs to $\mathcal{R}(T)$ or not. From Proposition 1 we know that the range of T is finite dimensional and that its dimension is $6m$, where m is the (unknown) number of buried scatterers. Thus we are in position to apply the MUSIC algorithm and define the orthogonal projection $P : L_t^2(\mathcal{E}; \mathbb{C}^3) \to \mathcal{R}(T)$ on this range and therewith the angle $\beta(\boldsymbol{y}) \in [0, \pi/2]$ between $\boldsymbol{g}_{y,d}$ and $\mathcal{R}(T)$ by

$$\cot \beta(\boldsymbol{y}) := \frac{\|P\boldsymbol{g}_{y,d}\|_{L^2(\mathcal{E};\mathbb{C}^3)}}{\|(I-P)\boldsymbol{g}_{y,d}\|_{L^2(\mathcal{E};\mathbb{C}^3)}}.$$

Here I denotes the identity operator. Then, by Proposition 2,

$$\boldsymbol{y} \in \{\boldsymbol{z}_1, \dots, \boldsymbol{z}_m\} \iff \beta(\boldsymbol{y}) = 0 \iff \cot \beta(\boldsymbol{y}) = \infty.$$

Using the measurement data at hand, we define for $l \in \mathbb{N}$ the orthogonal projections

$$P_l^\delta : L_t^2(\mathcal{E}; \mathbb{C}^3) \to \operatorname{span}_{\mathbb{C}}\{\boldsymbol{u}_1^\delta, \dots, \boldsymbol{u}_l^\delta\},$$

where $\boldsymbol{u}_1^\delta, \dots, \boldsymbol{u}_l^\delta$ are the left singular vectors corresponding to the l largest singular values of the operator A_δ from (9). Combining (17) with standard arguments from perturbation theory for linear operators, we find that for small values of δ the projection P is well approximated by the orthogonal projection P_{6m}^δ on the essential range of A_δ, spanned by $\boldsymbol{u}_1^\delta, \dots, \boldsymbol{u}_{6m}^\delta$ (see [20, pp. 83–84] and Kato [26] for details). Furthermore, (15) shows that in this case $\boldsymbol{g}_{y,d}$ is well approximated by $-\varepsilon_+/(k_+^2\varepsilon_-)F_\delta(\mathbb{G}_{k_-}(\,\cdot\,, \boldsymbol{y})\boldsymbol{d})$. Thus we define for $l \in \mathbb{N}$ the angle $\beta_l^\delta(\boldsymbol{y}) \in [0, \pi/2]$ by

$$\cot \beta_l^\delta(\boldsymbol{y}) := \frac{\|P_l^\delta F_\delta(\mathbb{G}_{k_-}(\,\cdot\,, \boldsymbol{y})\boldsymbol{d})\|_{L^2(\mathcal{E};\mathbb{C}^3)}}{\|(I-P_l^\delta)F_\delta(\mathbb{G}_{k_-}(\,\cdot\,, \boldsymbol{y})\boldsymbol{d})\|_{L^2(\mathcal{E};\mathbb{C}^3)}}. \tag{19}$$

Approximating $\cot \beta \approx \cot \beta_{6m}^\delta$, we expect that $\cot \beta_{6m}^\delta(\boldsymbol{y})$ has large values for test points $\boldsymbol{y}$ which are close to the points $\boldsymbol{z}_1, \dots, \boldsymbol{z}_m$. Hence, plots of $\cot \beta_{6m}^\delta$ can be used to visualize the positions of the scatterers.

Since the number scatterers $m \in \mathbb{N}$ is in general unknown, we follow [7, 21, 22] and visualize $\cot \beta_l^\delta$ from (19) for a sequence of increasing subspace dimensions $l = 6, 12, 18, \dots$. The cotangent $\cot \beta_l^\delta$ is monotonically increasing with l, and

typically the number of reconstructed scatterers is also increasing until all scatterers have been reconstructed.

7. **Numerical results.** In this section we present numerical results for the RG-MUSIC method and compare the reconstructions obtained with this algorithm to results of the standard MUSIC method from [21, 22] for the following example.

We consider a two-layered background medium as described in Section 2 with $\varepsilon_+ = \varepsilon_0 = 8.85 \cdot 10^{-12}\ \mathrm{Fm}^{-1}$, $\mu_+ = \mu_0 = 8.85 \cdot 10^{-12}\ \mathrm{Fm}^{-1}$, and

$$\varepsilon_- = \varepsilon_0\Big(\varepsilon_r + \mathrm{i}\,\frac{\sigma}{\omega\varepsilon_0}\Big) = (0.867 + \mathrm{i}\,59.5) \cdot 10^{-10}\ \mathrm{Fm}^{-1},$$
$$\mu_- = (1+\chi)\mu_0 = 1.26 \cdot 10^{-6}\ \mathrm{Hm}^{-1},$$

modeling air and soil, respectively. The particular electromagnetic soil parameters $\sigma = 7.5 \cdot 10^{-4}\ \mathrm{Sm}^{-1}$, $\chi = 1.9 \cdot 10^{-5}$, and $\varepsilon_r = 9.8$ refer to measurement data obtained by Igel and Preetz [25]. We suppose that two perfectly conducting ellipsoidal obstacles with semi axes of length $(0.5, 0.5, 1)\,\mathrm{cm}$ and $(1, 1.5, 2)\,\mathrm{cm}$, respectively, are buried in the lower half space. The centers of the two scatterers are at the positions $(-15, 15, -20)\,\mathrm{cm}$ and $(15, -15, -40)\,\mathrm{cm}$, respectively.

We consider incident fields that are imposed on an equidistant 6×6 grid $\mathcal{E}_h$ on a square $\mathcal{E}$ of size $0.5 \times 0.5\,\mathrm{m}^2$ parallel to the surface of ground with its center 0.1 m above the origin. To that end we apply magnetic dipoles with a frequency of 20 kHz and polarizations $\boldsymbol{e}_1$ and $\boldsymbol{e}_2$ at each of these grid points. Accordingly the wave numbers are $k_+ = 4.22 \cdot 10^{-4}\,\mathrm{m}^{-1}$ in air and $k_- = (7.77 + \mathrm{i}\,7.66) \cdot 10^{-3}\,\mathrm{m}^{-1}$ in soil, which corresponds to the wave lengths $\lambda_+ = 14.9\,\mathrm{km}$ and $\lambda_- = 0.81$ km. This gives 72 different incident fields.

To implement the RG-MUSIC algorithm described in the previous section, we need to approximate the operator A_δ from (9) and the test functions $F_\delta(\mathbb{G}_{k_-}(\cdot, \boldsymbol{y})\boldsymbol{d})$ from (8) for any test point $\boldsymbol{y}$ in the search domain. This amounts to approximating reciprocity gap functionals as defined in (6). Choosing the domain Ω large enough, taking into account the decay of the electromagnetic fields in the lower half space, we can restrict the integration over Γ in (6) to a bounded set contained in the surface of ground. We simulate the scattered electromagnetic fields for our example using the Nyström method for two-layered background media presented by Delbary et al. [16]. Since this solver does not give accurate results directly on the interface between the two layers, we evaluate the tangential components of the scattered and total electric and magnetic fields corresponding to the 72 incident fields on an equidistant 41×41 grid $\mathcal{M}_h$ on a square $\mathcal{M}$ of size $2 \times 2\,\mathrm{m}^2$ parallel to the surface of ground with its center 2 cm above the origin. Our numerical results show that the maximum of the absolute values of the total magnetic (resp. electric) fields on the boundary of $\mathcal{M}_h$ is approximately 1 % (resp. 2 %) of the maximum of the absolute values of the total magnetic (resp. electric) fields on $\mathcal{M}_h$. The scattered fields decay slightly slower.

To approximate the operator A_δ we compute $R(\boldsymbol{H}^s(\,\cdot\,; \boldsymbol{x}_j, \boldsymbol{e}_p), \mathbb{G}_{k_-}(\,\cdot\,, \boldsymbol{x}_l))$ for all $\boldsymbol{x}_j, \boldsymbol{x}_l \in \mathcal{E}_h$ and the two incident field polarizations $\boldsymbol{e}_1$ and $\boldsymbol{e}_2$. Then we approximate the integral appearing in the definition of the reciprocity gap functional (6) using the tensorial trapezoid quadrature rule on the measurement grid $\mathcal{M}_h$. This yields a (72×72)-dimensional matrix $A_{\delta,h}$ approximating the continuous operator A_δ.

Remark 2. Recalling the definition of the operator A_δ in (9), measurements of the total electric and magnetic fields on the measurement grid $\mathcal{M}_h$ should be sufficient

to approximate the operator A_δ. However, in view of (11), since for small scatterers as considered in this work the scattered fields on the measurement device are smaller by many orders of magnitude than the incident fields (in this example approximately by 6 orders of magnitude), this approximation is numerically unstable due to cancellation effects. Therefore, we use the scattered fields to approximate the operator A_δ, which means that in practice we would need to measure the tangential components of the scattered fields $\boldsymbol{e}_3 \times \boldsymbol{E}^s(\,\cdot\,;\boldsymbol{x}_j,\boldsymbol{e}_p)|_{\mathcal{M}_h}$ and $\boldsymbol{e}_3 \times \boldsymbol{H}^s(\,\cdot\,;\boldsymbol{x}_j,\boldsymbol{e}_p)|_{\mathcal{M}_h}$ as well as of the total fields $\boldsymbol{e}_3 \times \boldsymbol{E}(\,\cdot\,;\boldsymbol{x}_j,\boldsymbol{e}_p)|_{\mathcal{M}_h}$ and $\boldsymbol{e}_3 \times \boldsymbol{H}(\,\cdot\,;\boldsymbol{x}_j,\boldsymbol{e}_p)|_{\mathcal{M}_h}$ for all $\boldsymbol{x}_j \in \mathcal{E}_h$ and $p = 1, 2$.

As search domain we consider the cube $[-25,25]^2 \times [-50,-10]\,\mathrm{cm}^3$ underneath the center of the measurement device and approximate the cotangent $\cot\beta_{12}^\delta$ from (19) on an equidistant sampling grid with mesh width 0.5 cm. We choose $\boldsymbol{d} := \boldsymbol{e}_3$ as test dipole polarization and approximate for each test point $\boldsymbol{y}$ on this test grid the function $F_\delta(\mathbb{G}_{k-}(\,\cdot\,,\boldsymbol{y})\boldsymbol{d})$ on $\mathcal{E}_h$ using the tensorial trapezoid rule on $\mathcal{M}_h$ to compute the integral in the reciprocity gap functional. This yields a (72×1)-dimensional vector denoted by $\boldsymbol{g}_{y,d}^h$. Following [19], the left singular vectors of A_δ can be approximated by $D^{-1}\boldsymbol{u}_1^h, D^{-1}\boldsymbol{u}_2^h, \ldots$, where $\boldsymbol{u}_1^h, \boldsymbol{u}_2^h, \ldots$ are the left singular vectors of the matrix $A_{\delta,h}$ and D denotes the diagonal matrix whose entries are the weights of the tensorial trapezoid rule on $\mathcal{E}_h$. Thus, we approximate the indicator function $\cot\beta_{12}^\delta(\boldsymbol{y})$ from (19) by

$$\cot\beta_{12}^{\delta,h}(\boldsymbol{y}) := \left(\frac{\sum_{j\le 12} \left| \left(\boldsymbol{g}_{y,d}^h\right)^* D\boldsymbol{u}_j^h \right|}{\sum_{12<j<p} \left| \left(\boldsymbol{g}_{y,d}^h\right)^* D\boldsymbol{u}_j^h \right|} \right)^{1/2},$$

where $\left(\boldsymbol{g}_{y,d}^h\right)^*$ denotes the complex conjugated transpose of $\boldsymbol{g}_{y,d}^h$ and p is an integer smaller equal 72. Here we use $p = 30$, which gives good reconstructions but is computationally cheaper than, e.g., $p = 72$.

Remark 3. Recalling (16) measurements of the tangential components of the incident fields $\boldsymbol{e}_3 \times \boldsymbol{E}^i(\,\cdot\,;\boldsymbol{x}_j,\boldsymbol{e}_p)|_{\mathcal{M}_h}$ and $\boldsymbol{e}_3 \times \boldsymbol{H}^i(\,\cdot\,;\boldsymbol{x}_j,\boldsymbol{e}_p)|_{\mathcal{M}_h}$ instead of the total fields would also be enough to approximate the test functions $\boldsymbol{g}_{y,d}$ from (18).

The left hand plot in Figure 2 is a visualization of the reconstructed positions of the two scatterers obtained by the RG-MUSIC algorithm. It shows two isosurfaces of $\cot\beta_{12}^{\delta,h}$ and their orthogonal projections on the coordinate planes. To obtain an optimal spatial resolution in this visualization, we use different isosurfaces in different areas of the search domain. The isosurface corresponding to the upper obstacle corresponds to $\cot\beta_{12}^{\delta,h}(\boldsymbol{y}) = 0.72M$, whereas the other one uses the value $\cot\beta_{12}^{\delta,h}(\boldsymbol{y}) = 0.97M$. Here M denotes the maximum of $\cot\beta_{12}^{\delta,h}$ in the search domain. While the horizontal positions of the scatterers are nicely recovered, the reconstructed vertical positions are slightly too low. The right hand plot in Figure 2 shows the singular values of A_δ. From their super-linear decay we conclude that in the presence of noise the given data contain only very limited information on the scatterers.

Next we add 1 % equally distributed relative error to the simulated scattered fields and 1 % equally distributed relative error to the total fields to simulate measurement errors and use these data to recover the positions of the scatterers. The left hand plot in Figure 3 shows reconstructions obtained by the RG-MUSIC method. The isosurface corresponding to the upper obstacle corresponds to $\cot\beta_{12}^{\delta,h}(\boldsymbol{y}) = 0.98M$, whereas the other one uses the value $\cot\beta_{12}^{\delta,h}(\boldsymbol{y}) = 0.87M$ (the value of M differs

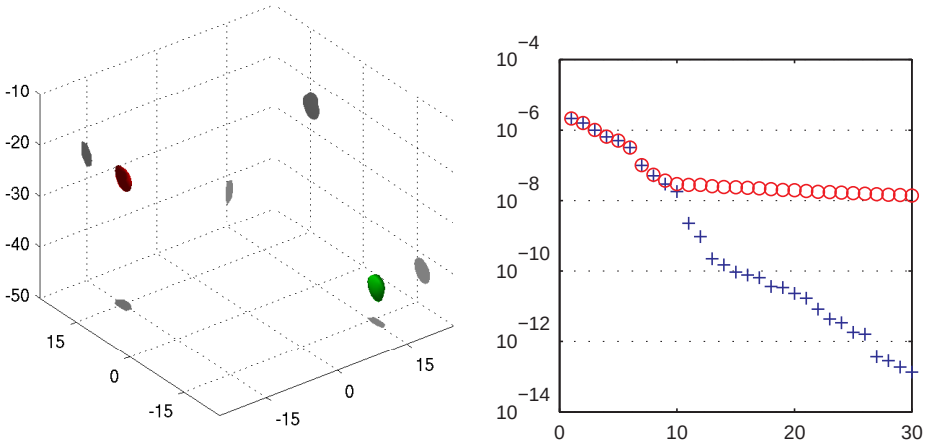

Figure 2. Reconstruction of the RG-MUSIC algorithm (left) and singular values of the operator A_δ (+ without additional noise, $\circ$ with 1 % uniformly distributed noise) (right).

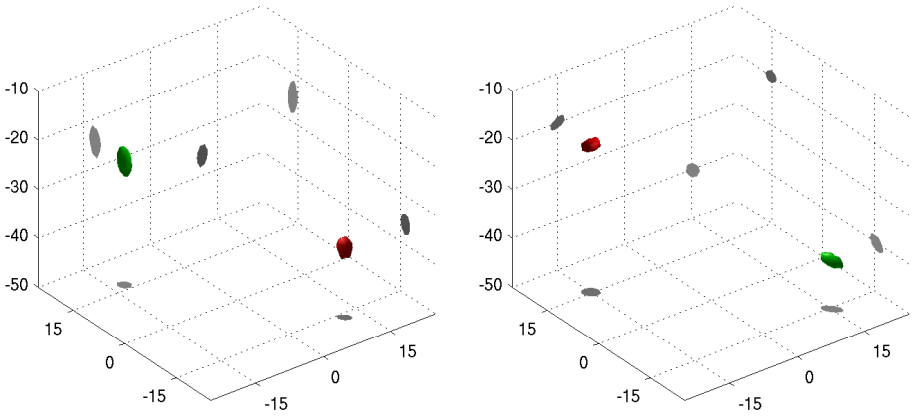

Figure 3. Reconstruction of the RG-MUSIC algorithm (left) vs. reconstruction of the standard MUSIC algorithm (right) with 1 % noise.

from above). The right hand plot in Figure 3 shows reconstructions obtained by the standard MUSIC method from [21, 22] using essentially the same setup and the same test dipole polarization $\boldsymbol{d} = \boldsymbol{e}_3$. This method requires measurements of the tangential components of the scattered magnetic field on the 6×6 grid $\mathcal{E}_h$ only, but it needs to evaluate the magnetic dyadic Green's function for the two-layered background medium for each test point $\boldsymbol{y}$ in the search domain (cf. [21, 22] for details). The forward data used by the standard MUSIC method are again computed using the Nyström method for the two-layered background medium from [16] and they are also perturbed by 1 % equally distributed relative error. The isosurface corresponding to the upper obstacle in this visualization uses $\cot \tilde{\beta}_{12}^{\delta} = 0.40\tilde{M}$, while the other one corresponds to $\cot \tilde{\beta}_{12}^{\delta} = 0.56\tilde{M}$. Here, $\cot \tilde{\beta}_{12}^{\delta}$ denotes

the indicator function of the standard MUSIC algorithm and $\tilde{M}$ is its maximum in the search domain.

Both methods detect the two objects at approximately the correct positions. The reconstructions of the positions obtained by the standard MUSIC method is slightly more accurate. On the other hand, the computation of the reconstruction using the RG-MUSIC method was 2.5 times faster for this example.

8. **Conclusions.** We have presented a modified MUSIC reconstruction method for an inverse scattering problem from subsurface imaging. Given multi-static measurements of electric and magnetic fields on the surface of ground this method can be used to reconstruct tiny objects buried in the ground, as long as the relevant information is above the inherent noise in the data. In contrast to standard MUSIC reconstruction methods our algorithm avoids the computation of the Green's function for the background medium. Therefore the method is much easier to implement and also slightly faster. However, the RG-MUSIC method as described here needs measurements of electric and magnetic scattered and total (or incident) fields, and for our particular example the reconstructed positions of the scatterers obtained by the standard MUSIC method from [21, 22] are slightly more accurate. Finally, we mention that the RG-MUSIC method can also be used for more complicated background media as long as the background medium is known inside the surface Γ enclosing the scatterers, i.e. in Ω.

Acknowledgments. We are grateful to Roland Potthast and his group for providing their codes from [16] to generate the forward data for the numerical examples, and to Christoph Schneider for his code for the Linear Sampling Method from [19], which has been adapted to implement the MUSIC methods presented here. The author also wants to thank Fioralba Cakoni, David Colton, Bastian Gebauer, and Peter Monk for inspiring and encouraging discussions.

REFERENCES

[1] H. Ammari, E. Iakovleva and H. Kang, *Reconstruction of a small inclusion in a two-dimensional open waveguide*, SIAM J. Appl. Math., **65** (2005), 2107–2127.

[2] H. Ammari, E. Iakovleva and D. Lesselier, *Two numerical methods for recovering small electromagnetic inclusions from scattering amplitude at a fixed frequency*, SIAM J. Sci. Comput., **27** (2005), 130–158.

[3] H. Ammari, E. Iakovleva and D. Lesselier, *A MUSIC algorithm for locating small inclusions buried in a half–space from the scattering amplitude at a fixed frequency*, Multiscale Model. Simul., **3** (2005), 597–628.

[4] H. Ammari, E. Iakovleva, D. Lesselier and G. Perrusson, *MUSIC–type electromagnetic imaging of a collection of small three–dimensional bounded inclusions*, SIAM J. Sci. Comput., **29** (2007), 674–709.

[5] H. Ammari and H. Kang, "Polarization and Moment Tensors with Applications to Inverse Problems and Effective Medium Theory," Appl. Math. Sci., vol. **162**, Springer–Verlag, Berlin, 2007.

[6] H. Ammari, M. S. Vogelius and D. Volkov, *Asymptotic formulas for perturbations in the electromagnetic fields due to the presence of inhomogeneities of small diameter II. The full Maxwell equations*, J. Math. Pures Appl., **80** (2001), 769–814.

[7] M. Brühl, M. Hanke and M. S. Vogelius, *A direct impedance tomography algorithm for locating small inhomogeneities*, Numer. Math., **93** (2003), 635–654.

[8] C. Bruschini, *Metal detectors in civil engineering and humanitarian demining: Overview and tests of a commercial visualizing system*, INSIGHT - Non-Destructive Testing and Condition Monitoring, **42** (2000), 89–97.

[9] F. Cakoni, M'B. Fares and H. Haddar, *Analysis of two linear sampling methods applied to electromagnetic imaging of buried objects*, Inverse Problems, **22** (2006), 845–867.

[10] A. Carruthers, M. Gaal, D. Guelle, K. Koppetsch, T. Lardner and C. Müller, "Metal Detectors and PPE Catalogue 2007," (J. Glattbach, ed.), Geneva International Centre for Humanitarian Demining (GICHD), Geneva, 2007.
[11] M. Cheney, *The linear sampling method and the MUSIC algorithm*, Inverse Problems, **17** (2001), 591–595.
[12] W. C. Chew, "Waves and Fields in Inhomogeneous Media," Van Nostrand Reinhold, New York, 1990.
[13] D. Colton and H. Haddar, *An application of the reciprocity gap functional to inverse scattering theory*, Inverse Problems, **21** (2005), 383–398.
[14] P.-M. Cutzach and C. Hazard, *Existence, uniqueness and analyticity properties for electromagnetic scattering in a two–layered medium*, Math. Methods Appl. Sci. **21** (1998), 433–461.
[15] G. Dassios and R. Kleinman, "Low Frequency Scattering," Oxford Math. Monogr., Oxford University Press, New York, 2000.
[16] F. Delbary, K. Erhard, R. Kress, R. Potthast and J. Schulz, *Inverse electromagnetic scattering in a two–layered medium with an application to mine detection*, Inverse Problems, **24** (2008), 015002 (18 pp.).
[17] A. J. Devaney, *Super–resolution processing of multi–static data using time reversal and MUSIC*, Preprint, Department of Electrical Engineering, Northeastern University, Boston, MA, (1999).
[18] A. Friedman and M. S. Vogelius, *Identification of small inhomogeneities of extreme conductivity by boundary measurements: A theorem on continuous dependence*, Arch. Rational Mech. Anal., **105** (1989), 299–326.
[19] B. Gebauer, M. Hanke, A. Kirsch, W. Muniz and C. Schneider, *A sampling method for detecting buried objects using electromagnetic scattering*, Inverse Problems, **21** (2005), 2035–2050.
[20] R. Griesmaier, "Detection of Small Buried Objects: Asymptotic Factorization and MUSIC," Dissertation, Johannes Gutenberg–Universität, Mainz, 2008, `http://nbn-resolving.de/urn/resolver.pl?urn=urn:nbn:de:hebis:77-16663`.
[21] R. Griesmaier, *An asymptotic factorization method for inverse electromagnetic scattering in layered media*, SIAM J. Appl. Math., **68** (2008), 1378–1403.
[22] R. Griesmaier and M. Hanke, *An asymptotic factorization method for inverse electromagnetic scattering in layered media II: A numerical study*, Contemp. Math., (2009), to appear.
[23] R. Griesmaier and M. Hanke, *MUSIC-characterization of small scatterers for normal measurement data*, Inverse Problems, **25** (2009), 075012 (12pp).
[24] E. Iakovleva, S. Gdoura, D. Lesselier and G. Perrusson, *Multistatic response matrix of a 3–D inclusion in half space and MUSIC imaging*, IEEE Trans. Antennas Propagat. **55** (2007), 2598–2609.
[25] J. Igel and H. Preetz, *Elektromagnetische Bodenparameter und ihre Abhängigkeit von den Bodeneigenschaften. — Zwischenbericht Projektverbund Humanitäres Minenräumen*, Technical Report, Leibniz Institute of Applied Geosciences, Hannover, (2005).
[26] T. Kato, "Perturbation Theory for Linear Operators," Grundlehren Math. Wiss., vol. **132**, Springer–Verlag, Berlin, 1966.
[27] A. Kirsch, *The MUSIC algorithm and the factorization method in inverse scattering theory for inhomogeneous media*, Inverse Problems, **18** (2002), 1025–1040.
[28] P. Monk, "Finite Element Methods for Maxwell's Equations," Numer. Math. Sci. Comput., Oxford University Press, New York, 2003.
[29] P. Monk and J. Sun, *Inverse scattering using finite elements and gap reciprocity*, Inverse Probl. Imaging, **1** (2007), 643–660.

Received March 2009; revised May 2009.

E-mail address: griesmai@math.udel.edu